Applied Catalysis B: Environmental 241 (2019) 205–216

Contents lists available at ScienceDirect

Applied Catalysis B: Environmental

journal homepage: www.elsevier.com/locate/apcatb

Insights into hydrothermal aging of phosphorus-poisoned Cu-SSZ-13 for NH_3-SCR

Kunpeng Xie[a], Jungwon Woo[a], Diana Bernin[a], Ashok Kumar[b], Krishna Kamasamudram[b], Louise Olsson[a,*]

[a] Competence Centre for Catalysis, Chemical Engineering, Chalmers University of Technology, Gothenburg, SE 412 96, Sweden
[b] Cummins Inc., 1900 McKinley Avenue, MC 50183, Columbus, IN 47201, USA

ARTICLE INFO

Keywords:
Cu/SSZ-13
Zeolites
Catalyst deactivation
Phosphorus-poisoning
Hydrothermal aging

ABSTRACT

Automotive catalysts are continuously exposed to different poisons and to high temperature, which result in hydrothermal aging. Phosphorus is one of the poisons that the catalyst could be exposed to and it originates from the lubricant oil. In this work, we study the influence of phosphorus poisoning on the catalytic performance and the deactivation mechanism in the hydrothermal aging of Cu-SSZ-13 catalysts. Phosphorus poisoning was performed by impregnating the Cu-SSZ-13 catalysts with $(NH_4)_2HPO_4$ solution using the incipient wetness impregnation method, which allowed us to precisely control the amount of phosphorus poison on the catalyst. XPS results show that phosphorus oxide (P_2O_5), metaphosphate (PO_3^-) and phosphate (PO_4^{3-}) are formed on the surface of phosphorus-poisoned catalysts, and metaphosphate is the main compound among those species. Phosphorus tends to interact with copper sites and strongly impacts the electronic and reduction property of Cu, as disclosed using EDX mapping, UV–vis DRS and H_2-TPR. Results of catalytic activities show that phosphorus poisoning is more severe on ammonia and NO oxidation reactions than on standard ammonia-SCR. This is possibly due to the formation of copper phosphates in the large cages, as revealed using H_2-TPR, which reduces the oxidation capacity. Moreover, results of XRD and ^{27}Al and ^{31}P solid-state NMR reveal that phosphorus not only interacts with copper by forming a P−O−Cu linkage but also partially inserts into the zeolite framework by forming a localized $AlPO_4$ phase. Both non-poisoned and P-poisoned catalysts lose their active sites and chabazite structures due to dealumination after successively aging in hydrothermal conditions (8 vol.% O_2, 5 vol.% H_2O in Ar) at different temperatures (800, 850, and 900 °C), which results in a large decrease in SCR performance. Specifically, the P-poisoned catalysts degrade faster than the non-poisoned catalysts. Results demonstrate that phosphorus induces the extensive formation of $AlPO_4$ that accelerates the dealumination during hydrothermal aging. This work provides new insight into understanding the deactivation mechanism in Cu-SSZ-13 from the perspectives of phosphorus-poisoning and hydrothermal aging, and it clearly shows that it is crucial to examine poisoning and hydrothermal aging simultaneously.

1. Introduction

Selective catalytic reduction with ammonia (NH_3-SCR) has been successfully developed as a promising technology for the removal of nitrogen oxides (NO_x) from the exhaust of stationary, automotive sources and municipal solid waste incinerators [1–4]. Cu-SSZ-13, which was discovered as an efficient and robust SCR catalyst by Bull et al. (BASF Catalyst LLC) in 2009 [5], has been extensively studied to gain a fundamental understanding of the active sites [6–14], the hydrothermal stability [15–20] and resistance to various poisons (e.g. metals [21,22], hydrocarbons [23,24], sulfur [25–28] and phosphorus [21,29]) in the exhaust stream.

Isolated monomeric Cu^{2+} and $[Cu^{II}(OH)]^+$ ions in Cu-SSZ-13 have been recognized as the active sites for NH_3-SCR [6,9–11]. While several recent studies demonstrate that a transient $[Cu^{I}(NH_3)_2]^+ - O_2 - [Cu^{I}(NH_3)_2]^+$ complex is the key intermediate during NH_3-SCR formed via a process of O_2 activation over $[Cu^{I}(NH_3)_2]^+$ species at low temperatures [11,12,30]. Copper ions have been demonstrated to possess dynamic characters that allow them to diffuse among the cages within the chabazite (CHA) framework under NH_3-SCR conditions [12,31]. In addition, Cu-SSZ-13 shows its superiority in hydrothermal stability under moderate aging

* Corresponding author.
E-mail address: louise.olsson@chalmers.se (L. Olsson).

https://doi.org/10.1016/j.apcatb.2018.08.082
Received 3 June 2018; Received in revised form 24 August 2018; Accepted 31 August 2018
Available online 05 September 2018
0926-3373/

temperatures (e.g. 750–800 °C) compared to other well-known Cu-zeolites (e.g. Cu-ZSM-5, Cu-beta and Cu-Y) [15], while it is less stable than LTA catalysts under harsh aging temperatures (i.e. 800–900 °C) [32,33]. Furthermore, Cu-SSZ-13 seems to be resistant to some poisons, such as Ca and Zn [21], as well as to hydrocarbons, e.g. propene [23,24], owing to its small-pore structure [14,21,24]. But it can be easily deactivated by sulfur, especially under NH_3-SCR conditions (NH_3 + NO + O_2 + H_2O) [25,28].

Lubricant oils (ZDDP) contain phosphorus, and it is, therefore, possible that catalysts are exposed to this [34], which would result in a deactivation of the catalyst. Few studies have been performed on phosphorus poisoning of Cu zeolites. Andonova et al. [35] have studied vapor-phase poisoning of Cu/BEA and found that the phosphorus was associated with the copper sites, since significantly more phosphorus was associated with the sample with a higher copper loading. There are very few studies available that examine phosphorus poisoning of Cu/SSZ-13. Lezcano-Gonzalez et al. observed a completely suppressing effect of P (2.2–8.8 wt.%) on Cu-SSZ-13 for standard SCR (0% conversion at 350 °C after poisoning) [21], while we previously observed a negligible impact of P (0.26–1.21 wt.%) on Cu-SSZ-13 for SCR reaction and an obvious poisoning effect on both ammonia oxidation and NO oxidation [29]. Therefore, more effort is still needed to reveal the phosphorus deactivation mechanism in SCR reaction.

With respect to the regeneration of poison-deactivated SCR catalysts, the simplest way is to regenerate them at high temperatures to remove/decompose the poisons, usually during the combustion of soot in the diesel particulate filter. Therefore, hydrothermal stability is vital to the practical use of Cu-SSZ-13 as SCR catalysts. There are several studies available examining hydrothermal stability using pure Cu-SSZ-13 catalysts [15,18,19,36]. However, evaluations of the influence of poisoning and hydrothermal stability have mostly been conducted separately. The influence of poisoning on Cu-SSZ-13 has been evaluated by a comparison of SCR activities before and after poisoning [21,24,25,28,29]. In one of our earlier studies, we examined the effect of sulfur poisoning on hydrothermally aged Cu/SSZ-13 and observed that more stable copper sulfates were formed [27].

Regeneration of phosphorus-poisoned catalysts is very difficult due to the high stability of phosphates [37,38]. Hydrothermally aging of P-poisoned catalysts might lead to structural changes of the catalyst supports, for example, the formation of $AlPO_4$ [39–41]. McCabe and coworkers have characterized the P-poisoned Pd three-way catalysts from high mileage taxis and observed the formation of $Zn_3(PO_4)_2$, $CePO_4$ and $AlPO_4$ [41]. Kanerva et al. have investigated the P poisoning of zeolite and oxide-supported Pt diesel oxidation catalysts by exposing them to a P-containing gas stream at 700 °C, and they observed the formation of $CePO_4$ and $AlPO_4$ [39]. Matam et al. have treated the Pd/Al_2O_3 three-way catalysts with $(NH_4)_3PO_4$ at a calcination temperature of 700 °C and found the formation of $AlPO_4$, which caused more deactivated Pd catalysts in three-way catalytic performance [40].

However, to our best knowledge, no study has reported on the influence of phosphorus on the hydrothermal stability of Cu-SSZ-13 under aging conditions above 750 °C, which is one of the objectives in the current study. In one of our earlier studies, we found that phosphates and metaphosphates were the main phosphorus species formed on gas phase poisoned Cu/BEA catalyst [35]. However, gas phase poisoning involves complex processes and also does not allow for a precise control of phosphorus loading on the catalysts. Therefore, impregnation with phosphates is considered as an alternative approach to poison the catalysts with exact amounts of phosphorus. Due to fact that ammonia is present in the SCR unit in the exhaust aftertreatment system, ammonia phosphates are very likely to be the dominant species. In this work, $(NH_4)_2HPO_4$ was therefore chosen as the poison precursor. Two P loadings (0.26 and 1.21 wt.%) were employed to avoid catalyst deactivation by physically blocking the pores. The influence of phosphorus on copper-active sites and the zeolite structure of fresh (non-poisoned and poisoned) and hydrothermally aged Cu-SSZ-13 catalysts was evaluated. Various characterization techniques were employed, such as X-ray photoelectron spectroscopy (XPS), scanning electron microscope (SEM) with energy-dispersive X-ray spectroscopy (EDX) mapping, UV–vis diffuse reflectance spectroscopy (UV–vis DRS), hydrogen temperature programmed reduction (H_2-TPR), diffuse reflectance infrared Fourier transform spectroscopy (DRIFTS), X-ray powder diffraction (XRD), and ^{27}Al and ^{31}P solid-state magic angle spinning nuclear magnetic resonance spectroscopies (ss-NMR). The catalysts were evaluated using several catalytic reactions, i.e. ammonia temperature-programmed desorption (NH_3-TPD), ammonia oxidation, NO oxidation and standard SCR.

2. Experimental methods

2.1. Zeolite synthesis and phosphorus poisoning

Non-poisoned and P-poisoned Cu-SSZ-13 (SAR (SiO_2/Al_2O_3) ratio of 12, Cu loading of 4.2 wt.%, and ion-exchange level of 0.33 Cu/Al) catalysts were prepared according to our previous work [29]. The non-poisoned Cu-SSZ-13 was notated as Cu_0 P. Theoretical P-poisoning levels of 0.1 and 0.4 mmol g^{-1} were investigated, and the resulting catalysts were notated as Cu_0.1 P and Cu_0.4 P, respectively. The phosphorus contents were determined to be 0.26 and 1.21 wt.%, respectively, as reported in our previous work [29]. The P loading corresponds to a P/Cu molar ratio of 0.13 and 0.59, but it should be noted that not all Cu will interact with the phosphorus as will be discussed in connection to the results.

2.2. Catalyst characterization

SEM images and EDX maps were acquired using an FEI Quanta 200 ESEM (Environmental SEM) coupled with an Oxford X-max 80 EDX detector. XRD was performed using a powder diffractometer (BrukerAXS D8 advance) with a nickel-filtered Cu Kα source (λ = 1.5418 Å) operating at 40 kV and 40 mA. XPS measurements were performed in a PerkinElmer PHI 5000C ESCA system, which was equipped with a monochromatic Al K αX-ray source (1486.6 eV, 12 kV, 22 mA) as incident radiation and a hemispherical energy analyzer. Charging effects were compensated using a flood gun. The base pressure in the measurement chamber was around 1×10^{-10} torr. The binding energies were calibrated using the C 1 s peak at 284.5 eV as an internal reference. For spectra deconvolution, a Shirley background, a Gaussian–Lorentzian mixed function with a ratio of 70:30, and an FWHM of 1.6 eV were applied for each component. UV–vis DRS was acquired in reflectance mode using an UV–vis-NIR spectrometer (Agilent Cary 5000) equipped with a diffuse reflectance attachment (DRA-2500 unit). The spectra were recorded in the 200–1500 nm wavelength range using $BaSO_4$ as the 100% reflectance standard.

H_2-TPR experiments were conducted in a digital scanning calorimeter (Setaram Sensys). Typically, about 60 mg of the powder sample (with grain size of 180–250 μm) was loaded in the reactor. A total flow rate of 20 ml min^{-1} was used for all the experiments. Prior to the reduction, the sample was degreened for 3 h at 500 °C by exposing it to a gas mixture containing 400 ppm NH_3, 8 vol.% O_2 in Ar and, subsequently, the sample was cleaned with 8 vol.% O_2 in Ar for 1 h at the same temperature before it was cooled to room temperature in the same gas flow. Thereafter, the feeding gas was switched to 0.3 vol.% H_2 in Ar. After stabilizing the flow for 10 min, the sample was heated to 800 °C at a ramp rate of 10 K min^{-1}. The concentration of H_2 in the outlet was monitored using a mass spectrometer (HIDEN, HPR-20 QUI).

DRIFTS measurements were carried out using a Bruker 70 FTIR spectrometer in the diffuse reflectance mode. The powder samples were placed in an in-situ flow cell (Harrick Praying Mantis DR accessory), which was covered by a dome equipped with three KBr windows. The total gas flow (reactant gas + Ar as balance) was kept constant at 200 ml min^{-1}. KBr was measured for the background of ex-situ IR

spectra. Each sample was pretreated with 8 vol.% O_2 in Ar for 30 min at 500 °C for dehydration and, subsequently, cooled to 30 °C in Ar flow. Thereafter, the spectrum was recorded using a scanner velocity of 20 kHz, a spectral resolution of 4 cm^{-1} and 64 scans. For in-situ IR spectra during NO adsorption, each sample was first pretreated with 8 vol.% O_2 in Ar for 30 min at 500 °C and, subsequently, cooled to 30 °C in Ar flow. A background was acquired after stabilization at 30 °C in Ar flow. Then the gas flow was switched to 500 ppm NO for 60 min. IR spectra were simultaneously acquired every 60 s using a scanner velocity of 20 kHz, a spectral resolution of 4 cm^{-1} and 64 scans.

Multinuclear ss-NMR experiments were performed using an Agilent Inova spectrometer (with a 1H Larmor frequency of –599.59 MHz) equipped with a 3.2 mm double-resonance MAS probe. All experiments were recorded at a MAS rate of 15 kHz. 1 M aqueous $Al(NO_3)_3$ and 85 wt% H_3PO_4 were used as an external chemical shift reference for the ^{27}Al and ^{31}P chemical shift scale, respectively. For quantitative ^{27}Al NMR spectra, a 10° radio frequency (rf) pulse calculated from the liquid 90° rf pulse of the reference solution was applied with a repetition delay of 3 s. The ^{27}Al background of the zirconia rotor was recorded by repeating the experiment with an empty rotor. For quantitative ^{31}P NMR spectra, a 90° rf pulse was applied with a repetition delay of 25 s A repetition delay of 3 s and a cross-polarization time of 1 ms were utilized for all Cross-Polarization (CP) experiments. All spectra were normalized by weight and the number of accumulated scans. Matlab (Mathworks) was employed to process the recorded time domain data using own scripts. A moderate Gaussian function was applied to the free induction decays prior to Fourier transformation.

2.3. Catalytic activity of monolith catalysts

For the catalytic tests, the powder catalysts were washcoated on monoliths (cordierite) following the detailed procedure described in our previous work [29,42]. The monoliths were in dimensions of 2 cm in length and 1.4 cm in diameter with a cell density of 400 cpsi. About 300 mg powder was used to washcoat each monolith. The resulting monolith catalysts were calcined in air at 500 °C for 2 h at a ramp rate of 5 K min^{-1}. For the flow reactor measurements, a total flow of 1200 ml min^{-1} (SV 22,100 h^{-1}) was maintained using Ar as the inert balance, and an MKS Multigas 2030 FTIR spectrometer was used to monitor the concentrations of gases (i.e. NH_3, NO, N_2O, NO_2 and H_2O). Before each reaction, the catalyst was pretreated with 8 vol.% O_2 and 5 vol.% H_2O in Ar for 20 min at 500 °C. In all experiments in the flow reactor water was present (5% H_2O), since it is always is present in real exhausts.

The standard NH_3-SCR experiments were performed by feeding the reactor with 400 ppm NH_3, 400 ppm NO, 8 vol.% O_2 and 5 vol.% H_2O in Ar. To determine the reaction rate of NO_x reduction for each catalyst, the reaction was first started at 80 °C and held for 2 h, thereafter the reactor was increased stepwise up to 150 °C at a ramp rate of 20 K min^{-1} between each step, and the duration per step was 1 h.

The NH_3 oxidation experiments were performed by exposing the catalysts to 400 ppm NH_3, 8 vol.% O_2 and 5 vol.% H_2O in Ar for 1 h at 200 °C and then increasing the temperature stepwise up to 280 °C at a ramp rate of 20 K min^{-1} between each step. The duration per step was also 1 h for these experiments.

The NO oxidation experiments were performed by exposing the catalysts to 400 ppm NO, 8 vol.% O_2 and 5 vol.% H_2O in Ar for 1 h at 200 °C and then increasing the temperature stepwise up to 500 °C at a ramp rate of 20 K min^{-1} between each step. The duration per step was also 1 h for these experiments.

For NH_3-TPD experiments, the monolith catalysts were first exposed to ammonia (400 ppm NH_3 and 5 vol.% H_2O in Ar) for 2 h at 100 °C, followed by purging with 5 vol.% H_2O in Ar for 1 h at the same temperature, and, subsequently, the catalysts were heated from 100 °C to 500 °C (at 10 K min^{-1}) with the same gas flow and maintained at 500 °C for 20 min before cooling.

2.4. Hydrothermal stability

The standard NH_3-SCR from 100 to 500 °C was again measured before the aging experiments were conducted. Schmieg, et al. [43], demonstrated that the loss of SCR activity of a Cu-CHA catalyst after accelerated hydrothermal aging (HTA) at higher temperatures with shorter durations compares with that after HTA at lower temperatures with longer durations. We therefore performed an accelerated HTA of the catalysts under severe conditions: the catalyst was hydrothermally aged (8 vol.% O_2, 5 vol.% H_2O and Ar balance) at 800, 850 and 900 °C with a duration of 4 h for each temperature step. This procedure was adapted from an accelerated HTA protocol developed by Luo, et al. [44], where Cu-SSZ-13 was progressively aged from 550 °C to 900 °C with a 50 °C increment and a duration of 4 h per step. After each aging step, the reactor was cooled to 100 °C in the same gas flow. Then the activity of standard NH_3-SCR from 100 to 500 °C was measured again. The successive procedure of such an SCR-Aging-SCR cycle is shown in Fig. S1 in Supplementary Materials. The catalysts before and after HTA aging are referred to as “fresh” and “aged” catalysts, respectively. After the last catalytic tests, small amounts of the powder of aged catalysts were scratched carefully from the monolith channels for further characterization.

3. Results and discussion

3.1. Characterization and catalytic activity of P-poisoned catalysts

XP survey spectra were recorded to identify the chemical composition of the surfaces of the non-poisoned and P-poisoned Cu-SSZ-13 samples (Fig. S2). All the spectra exhibited O 1 s, C 1 s, Al 2 s, Al 2p, Si 2 s, Si 2p peaks and Cu 2p peaks. P 2 s and P 2p peaks were only found on the surfaces of poisoned Cu-SSZ-13 samples. The intensities of P 2 s and P 2p peaks increased with P-poisoning level. The surface phosphorus contents were determined to be 2.4 and 5.0 at.% for Cu_0.1 P and Cu_0.4 P, respectively. Detailed XP P 2p spectra of P-poisoned Cu-SSZ-13 samples are shown in Fig. 1a. The XP P 2p spectrum of non-poisoned Cu-SSZ-13 was also measured for comparison and no peak was observed. There was a clear peak shift on the P 2p spectra caused by an increase in the level of P poisoning. The center of the peak was at around 135 eV for Cu_0.1 P while it shifted to 134 eV for Cu_0.4 P. The spectra of P 2p could be deconvoluted into three phosphorus species: phosphorus oxide (P_2O_5) at around 135.6 eV, metaphosphate (PO_3^-) at around 134.5 eV and phosphate (PO_4^{3-}) at around 133.2 eV [45]. The relative concentrations of the three phosphorus compounds were calculated for comparison and are presented in Fig. 1b. Metaphosphate was identified as the dominant phosphorus species for the poisoned sample with a high P loading, which is consistent with the literature, where “glassy” metaphosphates have often been observed on P-poisoned automotive catalysts [41,46]. Interestingly, when the P-poisoning level was as low as 0.1 mmol g^{-1} (Cu_0.1 P), phosphorus tended to form phosphorus oxide (44%) and metaphosphate (42%). Increasing the level of P poisoning to 0.4 mmol g^{-1} (Cu_0.4 P) resulted in a decrease in the amount of phosphorus oxide and an increase in metaphosphates and phosphates (P_2O_5: 44% → 23%; metaphosphate: 42% → 55%; phosphates 14% → 22%).

EDX mapping was performed under SEM observation to examine the distributions of elements (Al, Si, Cu and P) on P-poisoned Cu-SSZ-13 grains, as shown in Fig. 2. Note that the scale of the measurements was around 300 μm; each image included many Cu/SSZ-13 particles. Al and Si mappings showed uniform distributions, while Cu and P mappings both displayed several Cu-rich and P-rich areas. The P-rich areas well overlapped the Cu-rich areas. In addition, P and Al were found to match each other in several areas in the mappings, as marked by white arrows. These observations are further confirmed by the corresponding EDX line scans profiles. A good match of Al $K\alpha_1$ and P $K\alpha_1$ could be seen on the boundaries of particle grains, while a good match of Cu $K\alpha_1$ and P

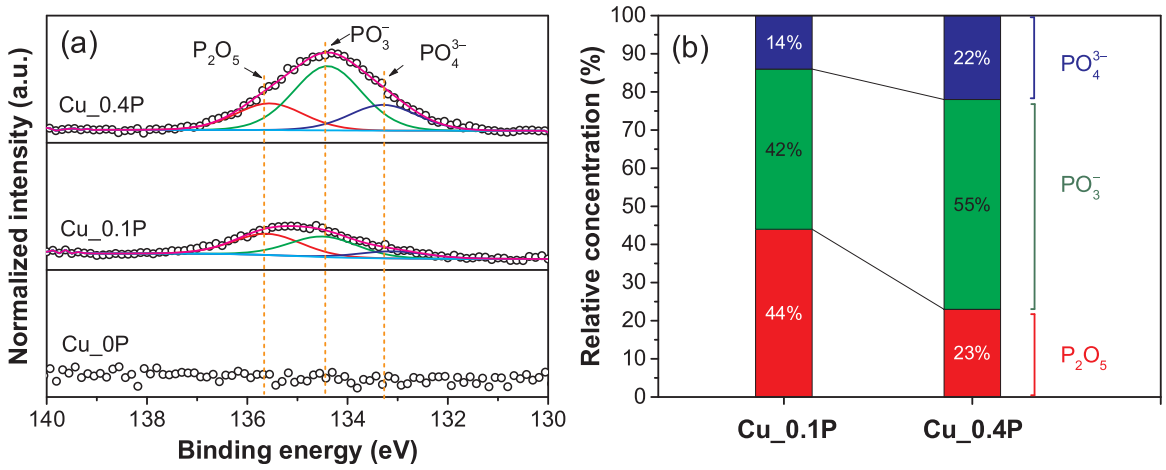

Fig. 1. (a) XP P 2p spectra of Cu_0 P, Cu_0.1 P and Cu_0.4 P. (b) The correspondingly relative concentrations of three phosphorus compounds obtained using spectral deconvolution.

$K\alpha_1$ could be seen in the bulk of particle grains, especially on Cu_0.4 P sample. The results of element mapping and line scans suggest that P species not only interacted with Cu species but also linked to zeolite framework.

The influence of phosphorus on the electronic transitions of Cu in the zeolite was probed with UV–vis DRS (Fig. 3). The UV–vis spectra of the non-poisoned and P-poisoned Cu-SSZ-13 show absorption bands in two major regions: 45,000–25,000 cm^{-1} (222–400 nm) and 15,000–10,000 cm^{-1} (667–1000 nm). In the former region, two absorption bands (marked as 1 and 2) are associated with the charge-transfer transitions from lattice oxygen (O^{2-}) to isolated Cu^{2+} ions [47]. Another two absorption bands in the later regions (marked as 3 and 4) are original from the characteristic d-d transitions of octahedrally coordinated copper (II) and tetrahedrally coordinated copper (II) [47,48]. Our earlier studies using reference materials, showed that CuO has clear intensity in the region 400–600 nm [27,49], which $Cu(OH)_2$ do not have. The region of 25,000–17,500 cm^{-1} (400–570 nm) is therefore used in our experiments to evaluate the existence for CuO [27,47,49]. The low absorbance in this region indicates that there are no or only minor amounts of CuO particles or clusters on both non-poisoned and P-poisoned samples. A 4-peak fitting was employed to deconvolute UV–vis spectra. It can be seen in Fig. 3b that the absorption centers of band 2, 3 and 4 on P-impregnated Cu-SSZ-13 have shifted to lower wavenumbers, and the peak intensities of 2 and 3 are enhanced on P-poisoned samples compared to those on non-poisoned Cu-SSZ-13. This finding demonstrates that the d-d transition processes in Cu^{2+} ions, and the charge transfer processes of $O^{2-} \rightarrow Cu^{2+}$ are strongly affected by phosphorus species, very likely due to the formation of copper phosphorus compounds.

H_2-TPR was employed to further probe the interaction between phosphorus and copper ions, and the results are shown in Fig. 4 and Table 1. Prior to the H_2-TPR, all the samples were degreened with 400 ppm NH_3, 8 vol.% O_2 in Ar for 3 h at 500 °C, and then the samples were cleaned with 8 vol.% O_2 for 1 h at the same temperature to ensure that the majority of the copper ions were in Cu^{2+} state. Cu_0 P shows two typical reduction peaks (marked as 1 and 2) in low temperature

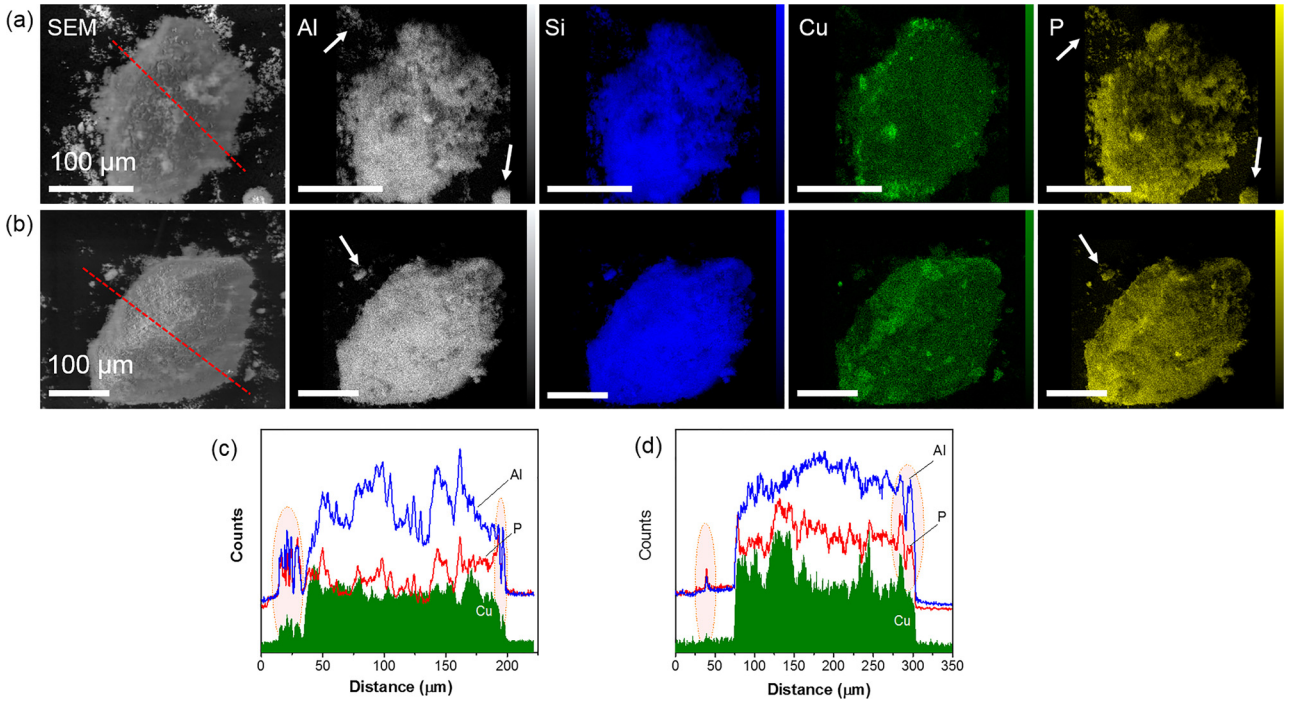

Fig. 2. SEM-EDX element mapping of (a) Cu_0.1 P and (b) Cu_0.4 P. EDX line scans for Cu $K\alpha_1$ and P $K\alpha_1$ on (c) Cu_0.1 P and (d) Cu_0.4 P, as indicated in SEM images.

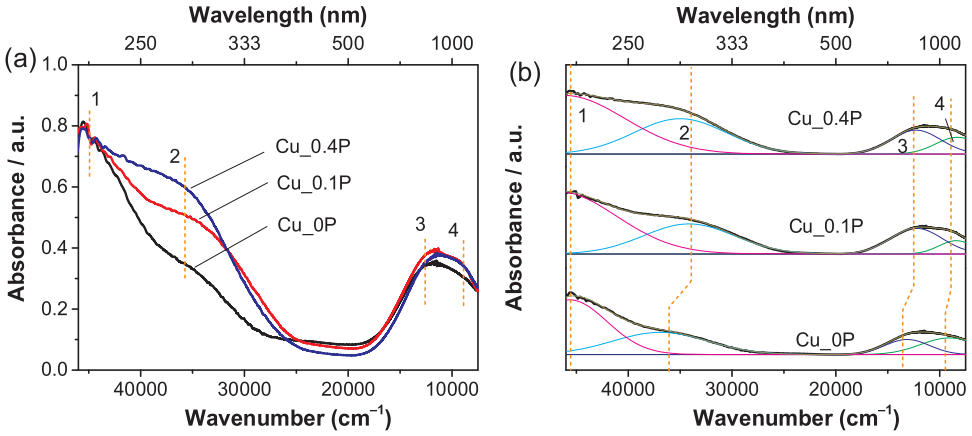

Fig. 3. (a) UV–vis spectra of Cu_0 P, Cu_0.1 P, and Cu_0.4 P. (b) The corresponding deconvolution of the spectra with 4 peaks.

regions, which is consistent with observations in the literature [20,50]. To exclude the possibility that H_2 consumption is from reaction with SSZ-13 itself, H_2-TPR of H-form SSZ-13 was measured, and no H_2 consumption was observed (Fig. S3), which means that the reduction peaks on Cu_0 P were only contributed by the copper reduction (Eqs. 1 − 3). Further, the reduction of Cu^+ to Cu^0 (Eq. (2)) in non-poisoned Cu-SSZ-13 requires temperatures higher than 800 °C, as reported in the literature [20,28,51]. To further confirm this point, the total H_2 consumption of Cu_0 P was calculated by integrating the H_2 consumption profile and referenced to copper content, resulting in a Cu/H_2 ratio of 2.04 for non-poisoned Cu-SSZ-13 (Table 1). This finding indicates that the entire consumption of H_2 on non-poisoned Cu-SSZ-13 is only contributed to by the one-electron reduction of Cu^{2+} to Cu^+ (Eq. (1)).

$$2Cu^{2+} + H_2 \rightarrow 2Cu^+ + 2H^+ \quad (1)$$

$$2Cu^+ + H_2 \rightarrow 2Cu^0 + 2H^+ \quad (2)$$

$$Cu^{2+} + H_2 \rightarrow Cu^0 + 2H^+ \quad (3)$$

After poisoning with P, two new reduction peaks (marked as 3 and 4) were clearly observed at higher temperatures, which can possibly be explained by the reduction of copper associated with phosphates/metaphosphates, as disclosed by the XPS studies. Similar phenomena have also been reported by Escalona et al. [52] and Mamontov et al. [53] when studying H_2-TPR over P_2O_5-modified Cu/SiO_2 catalysts. Furthermore, the Cu/H_2 ratios for the P-poisoned Cu-SSZ-13 decrease with the increase of the level of P poisoning, which indicates an additional reduction of Cu^+ to Cu^0 (Eq. (2)). Another possible explanation for the increase in hydrogen consumption could be a reduction of the phosphates/metaphosphates. In order to examine this possibility, an H/SSZ-13 sample was impregnated with phosphorus and studied in an H_2-TPR experiment (see Fig. S3). However, no hydrogen consumption was observed, which suggests that no hydrogen was consumed due to a reduction of the phosphates/metaphosphates. We can, therefore, conclude that the increase in hydrogen consumption for the phosphorus poisoned Cu/SSZ-13 is due to an increase in the reduction of copper species.

Table 1
P contents, Cu contents and consumption of H_2 (ΔH_2) for the non-poisoned and P-poisoned Cu-SSZ-13 catalysts.

	Cu content / μmol g^{-1}	ΔH_2 / μmol g^{-1}				Estimated percentage of Cu that interacts with P[b]
		Total	Cu/H_2 ratio	$Cu^{2+}\rightarrow Cu^+$	$Cu^+\rightarrow Cu^0$[a]	
Cu_0 P	664.6	325.4	2.04	325.4	–	
Cu_0.1 P	664.6	404.6	1.64	325.4	79.2	24%
Cu_0.4 P	658.3	477.5	1.38	325.4	152.1	46%

[a] [ΔH_2 ($Cu^+\rightarrow Cu^0$)] = [Total ΔH_2]–[ΔH_2 ($Cu^{2+}\rightarrow Cu^+$)].
[b] [Estimated percentage of Cu that interacts with P] = [2 × ΔH_2 ($Cu^+\rightarrow Cu^0$)] × 100%/[Cu content].

The consumption of H_2 by Cu^{2+} to Cu^+ and Cu^+ to Cu^0 is calculated and summarized in Table 1. It was found that phosphorus seems to facilitate the Cu^+ to Cu^0 as the consumption of H_2 by Cu^+ to Cu^0 increases with phosphorus loading and is above the ratio of 0.5 for H_2/Cu. Because of the minor difference in the copper content of the non-poisoned and P-poisoned catalysts, the consumption of H_2 by the Cu^{2+} to Cu^+ on Cu_0.1 P and Cu_0.4 P catalysts can be assumed to be the

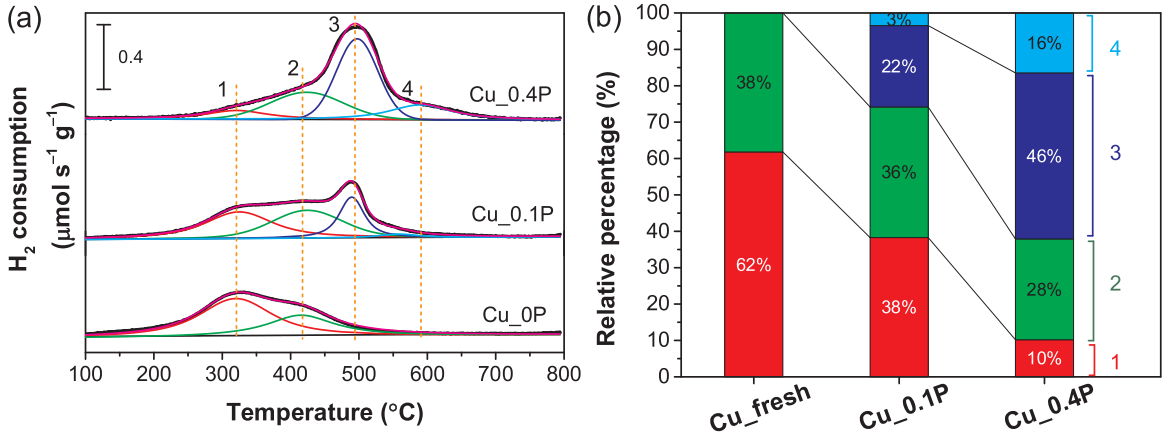

Fig. 4. (a) H_2-TPR profiles of Cu_0 P, Cu_0.1 P, and Cu_0.4 P (ramp: 10 K min^{-1}). (b) Calculated percentages of the reduction peaks for Cu_0 P, Cu_0.1 P and Cu_0.4 P.

same as for the Cu_0 P catalyst (Table 1). The results show, that Cu_0 P catalyst only has Cu^{2+} to Cu^{+} reduction reaction while Cu_0.1 P and Cu_0.4 P have Cu^{2+} to Cu^{+} and Cu^{+} to Cu^{0} reduction reactions. These results indicate that only the Cu^{2+} ions that interact with phosphorus can eventually be reduced to Cu^{0}, although it is difficult to distinguish whether the reduction path follows a two-step reduction (Eqs. (1), (2)) or a one-step reduction (Eq. (3)). Therefore, an estimation of the relative percentages of copper in the interaction with phosphorus was calculated, and the percentages were 24% and 46% for Cu_0.1 P and Cu_0.4 P, respectively. Note that the factor of the increase in the relative percentage of copper that interacts with P is near 2, which does not correlate with the factor of the increase in the level of P poisoning (i.e. 4, from 0.1 to 0.4). This suggests that the increase in the level of P poisoning limits the accessibility of copper to phosphorus. This is likely due to the blocking effect caused by the formation of phosphates/metaphosphates inside the pores.

With respect to the peak assignment for the H_2-TPR profile of the non-poisoned Cu-SSZ-13, it is generally recognized that the peaks in higher and lower temperature regions can be assigned to the Cu^{2+} ions close to the six-membered rings (6-MRs) and eight-membered rings (8-MRs), respectively [50,54]. It should be noted that during SCR conditions the copper is solvated and mobilized, which was presented by Paolucci et al. [55] based on XAS and ab-initio calculations. However, during ex-situ conditions the copper is positioned in the 6- and 8-MRs [55], and this is the case in H_2-TPR conditions. In our study, H_2-TPR could give interesting information relating to where in the structure the phosphorus is positioned. Following the assignment of 6- and 8-MRs [50,54], the TPR profile of Cu_0 P can be deconvoluted into two peaks: peak 1 at around 320 °C for Cu^{2+} ions close to 8-MRs (62%) and peak 2 at around 420 °C for Cu^{2+} ions close to 6-MRs (38%). The H_2-TPR profiles of Cu_0.1 P and Cu_0.4 P were deconvoluted using a four-peak fitting by taking into consideration two new reduction peaks centered at around 490 °C and 580 °C. The relative percentages of the reduction peaks for each sample are summarized and plotted in Fig. 4b. It can be seen in the figure that the decrease in the relative percentage of Cu^{2+} ions close to 8-MRs is much more dramatic than that of Cu^{2+} ions close to 6-MRs as the phosphorus loading is increasing. This implies that phosphorus tends to interact with the Cu^{2+} ions close to 8-MRs rather than those close to 6-MRs. This is reasonable when considering the fact that there is less sterical hindrance in the large cages (8-MRs).

Powder catalysts were washcoated on monoliths to evaluate the catalytic activity. It is well known that there are many side reactions that occur during standard NH_3-SCR, especially NH_3 oxidation, which strongly impact the efficiency of NO_x reduction at high temperatures. NO oxidation was also studied as a model reaction to understand more about the impact of phosphorus on oxidation functions. Ammonia storage is also a key factor for NO_x reduction in transient cycles. NH_3-TPD is commonly performed to determine the NH_3 storage on both Lewis acidic sites and Brønsted acidic (H^+) sites. The reactions were performed in the order NH_3-SCR, NH_3 oxidation, NO oxidation, and NH_3-TPD, and between each reaction the catalyst was pre-treated at 500 °C with 8 vol.% O_2, 5 vol.% H_2O and Ar balance.

The NH_3-TPD profiles show that the overall ammonia storage of poisoned catalysts decreases with an increase in the level of P poisoning (Fig. 5a), which indicates a negative effect of phosphorus on NH_3 storage in a Cu-SSZ-13 catalyst. Three NH_3 desorption peaks were identified according to the procedure in our previous work. The S1 peak (306–317 °C), S2 peak (407–421 °C) and S3 peak (212–219 °C) were assigned to the moderately bound NH_3, the strongly bound NH_3 and the weakly bound NH_3, respectively [56]. Peak fitting was performed on the NH_3 desorption profiles using the Gaussian function, and the fitting of the NH_3 desorption profile of Cu_0 P is shown as an example in Fig. 5a. The overall amount of desorbed ammonia and three individual amounts of the desorbed ammonia for each catalyst were calculated and plotted as a function of the level of P poisoning, as shown in Fig. 5b. Increasing the level of P poisoning led to descending ammonia storages

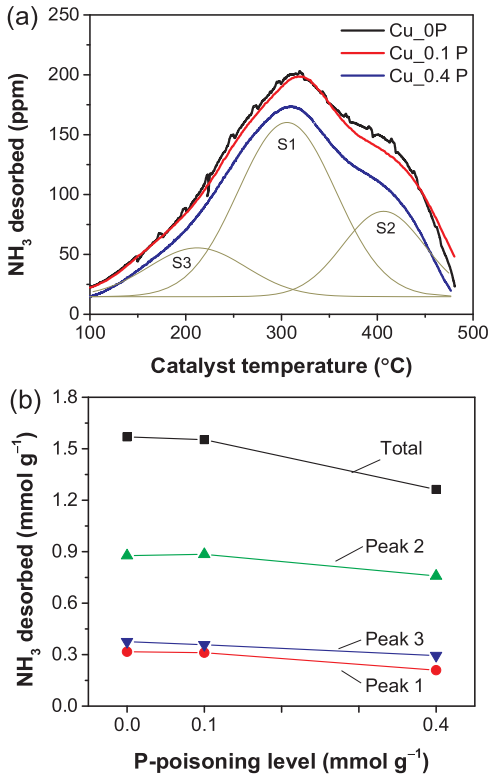

Fig. 5. (a) NH_3-TPD profiles of Cu_0 P, Cu_0.1 P and Cu_0.4 P. Peak fitting is shown for Cu_0 P as an example. (b) NH_3 desorption as a function of level of P poisoning.

on S1, S2 and S3 and an overall decrease in ammonia storage. This result is consistent with Andonova's work, where a similar negative effect of P was observed when Cu/BEA catalysts were poisoned with H_3PO_4 vapor [35]. It was also noticed that this result differs from the case of sulfur poisoning reported in our previous work, where increased NH_3 storages were observed on S-poisoned Cu-SSZ-13 catalysts [28].

In our previous study, we found that phosphorus had severely negative effects on ammonia oxidation and NO oxidation, while its impact on standard SCR reaction was nearly negligible when the reaction temperature was below 300 °C [29]. To further understand the influence of phosphorus on those reactions (i.e. ammonia oxidation, NO oxidation and NH_3-SCR), the results at low conversions were used to determine reaction rates. The results are shown in Fig. 6 and Table 2.

NH_3 oxidation on non-poisoned and P-poisoned Cu-SSZ-13 catalysts was examined, resulting in steady-state conversions of NH_3 oxidation between 3.2% and 9.8% (for the temperature 206–237 °C), as shown in Table 2. The influence of level of P Poisoning on the reaction rate is depicted by taking the oxidation temperature at around 215 °C as an example (Insert of Fig. 6a). The reaction rate of NH_3 oxidation decreased with P level, which was probably due to the strong interaction between phosphorus and copper sites for NH_3 oxidation. Fig. 6a displays the Arrhenius plots for non-poisoned and P-poisoned Cu-SSZ-13 catalysts. The more phosphorus loaded on a catalyst, the lower the reaction rate obtained. This trend was observed at different temperatures. The derived activation energies are listed in Table 2. The activation energy was about 65.9 kJ mol^{-1} for Cu_0 P, which is consistent with our previous findings [56], where ammonia oxidation that occurred at low temperatures exhibited low activation energy (E_a: 72.7 kJ mol^{-1}). The activation energies for P-poisoned Cu-SSZ-13 catalysts were found to be slightly higher than Cu_0 P, which indicates that phosphorus influences the NH_3 oxidation on copper sites.

NO oxidation was also investigated and resulted in steady-state conversions of NO oxidation between 1.7% and 11.2% (for

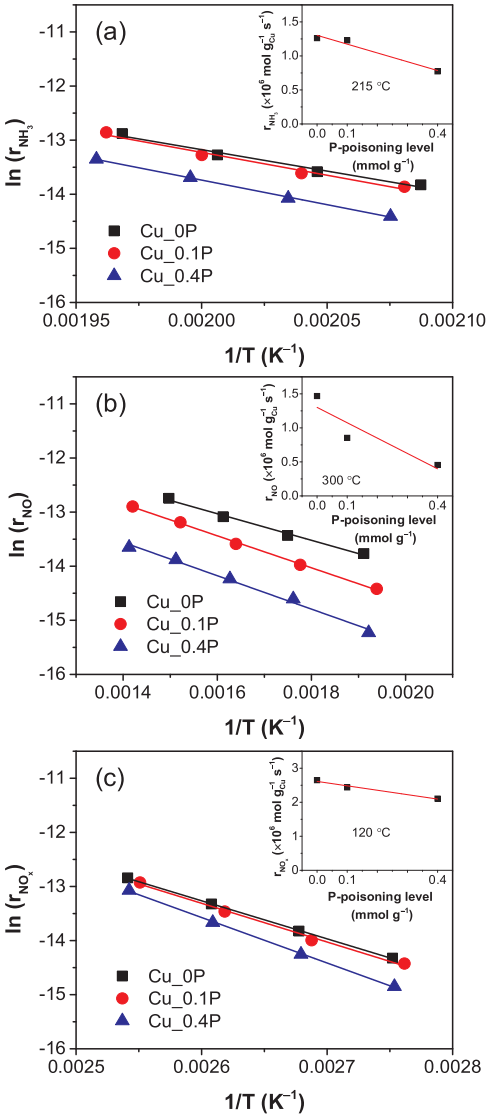

Fig. 6. Arrhenius plots for Cu_0 P, Cu_0.1 P and Cu_0.4 P in the reactions: (a) NH_3 oxidation from 206 to 237 °C (Insert: effect of P level on the NH_3 oxidation reaction rate at around 215 °C), (b) NO oxidation from 243 to 437 °C (Insert: effect of P level on the reaction rate of NO oxidation at around 300 °C), and (c) NH_3-SCR from 90 to 120 °C (Insert: effect of P level on the reaction rate of NO_x reduction at around 120 °C).

Table 2
Calculated activation energy (E_a) from Arrhenius plots over non-poisoned and P-poisoned Cu-SSZ-13 samples.

Reaction	Catalyst	Catalyst temperature region (°C)	Conversion range (%)	E_a (kJ mol^{-1})
NH_3 oxidation	Cu_0P	206–235	3.8–9.8	65.9
	Cu_0.1 P	207–236	3.5–9.6	70.3
	Cu_0.4 P	209–237	3.8–6.2	75.6
NO oxidation	Cu_0P	250–395	4.0–11.2	20.4
	Cu_0.1 P	243–431	2.0–9.2	24.6
	Cu_0.4 P	247–435	1.7–5.4	25.6
NH_3-SCR	Cu_0P	90–120	2.3–10.1	58.5
	Cu_0.1 P	89–119	2.0–8.9	59.5
	Cu_0.4 P	90–120	1.4–8.3	69.9

temperatures in the range of 243–435 °C), as shown in Table 2. The influence of level of P poisoning on the reaction rate is shown with the oxidation temperature at around 300 °C as an example (Insert of Fig. 6b). Similar to the observation on NH_3 oxidation, the reaction rate of NO oxidation decreased with P level. The Arrhenius plots for non-poisoned and P-poisoned Cu-SSZ-13 catalysts are presented in Fig. 6b. The reaction rate of NO oxidation declined with level of P poisoning at different reaction temperatures. The activation energies derived from Arrhenius plots are listed in Table 2. The activation energy of Cu_0.4 P (25.6 kJ mol^{-1}) was also slightly higher than that of Cu_0 P (20.4 kJ mol^{-1}). The active sites for NO oxidation are commonly assigned to the Cu_xO_y oligomers located in the large cages inside Cu-SSZ-13 [57]. Therefore, the suppressed reaction rate of NO oxidation over P-poisoned Cu-SSZ-13 catalysts could be related to the loss of Cu_xO_y oligomers due to the formation of copper phosphates in the large cages, as disclosed in the H_2-TPR study.

Standard NH_3-SCR for non-poisoned and P-poisoned Cu-SSZ-13 catalysts was examined and resulted in steady-state conversions of NO_x reduction between 1.4% and 10.1% (for temperatures in the range of 89–120 °C), as shown in Table 2. As NO oxidation was nearly inactive in this temperature region, the NO_x conversion was almost equal to NO conversion. The reaction rate as a function of P level at around 120 °C is shown as an example in the insert of Fig. 6c. The corresponding Arrhenius plots for fresh and P-poisoned Cu-SSZ-13 catalysts are presented in Fig. 6c. The activation energies derived from Arrhenius plots are listed in Table 2. The reaction rate of NO_x reduction decreased with level of P poisoning and the activation energy slightly increased with level of P poisoning. However, it should be noted that the decrease in NO_x conversions on the P-poisoned catalysts was very small compared to the non-poisoned catalyst, which differs from observations of NH_3 and NO oxidation. Therefore, the influence of phosphorus on NO_x reduction in the low temperature region is minor, but there is a clear trend of increasing activation energy.

3.2. Hydrothermal aging of P-poisoned catalysts

An SCR catalyst is exposed to hydrothermal conditions also after it has been poisoned from various species. Therefore, it is essential to study the influence of poisons on the hydrothermal stability of SCR catalysts. We investigated the SCR activities of non-poisoned and P-poisoned Cu-SSZ-13 monolith catalysts by successively aging them at 800, 850 and 900 °C. The NO_x conversion of the catalysts before aging ("fresh") and after aging ("aged") at different temperatures are shown in Fig. 7. The NO_x conversions of all fresh catalysts increased from near 0% to near 100% as the reaction temperature increased from 100 °C to 200 °C, and held at 100% between 250 °C and 300 °C (Fig. 7a). Fresh non-poisoned and P-poisoned Cu-SSZ-13 catalysts showed similar activities in the reaction temperature region below 300 °C. For the reaction temperatures above 300 °C, the fresh P-poisoned catalysts had a higher NO_x conversion than fresh non-poisoned catalysts. The reason for this is because the ammonia oxidation rate was reduced to a larger extent than that of NH_3-SCR, which affected the NO_x selectivity [29]. We have previously observed this effect for hydrothermally aged Cu/BEA [58].

Our results for H_2-TPR clearly show that phosphorus severely impacts the reduction capabilities of copper, and in addition there is a clear poisoning effect for ammonia and NO oxidation. After hydrothermally aging at 800 °C, 850 °C and 900 °C, the NO_x conversion for all the catalysts gradually decreased. NO_x conversions of aged P-poisoned catalysts dropped more significantly than those of aged non-poisoned catalysts. The loss of NO_x conversion depended on the level of P poisoning, which indicates that P poisoning induced a faster catalyst deactivation during hydrothermal aging. These results clearly show that it is important to study chemical poisoning and hydrothermal aging simultaneously. In addition, it was found that the ammonia uptakes for non-poisoned and P-poisoned catalysts decreased with increasing aging temperature (Fig. S4a-b)). The summary of total ammonia uptakes shows that aged P-poisoned catalysts degrade faster than aged non-poisoned catalysts, and the degradation depends on the level of P

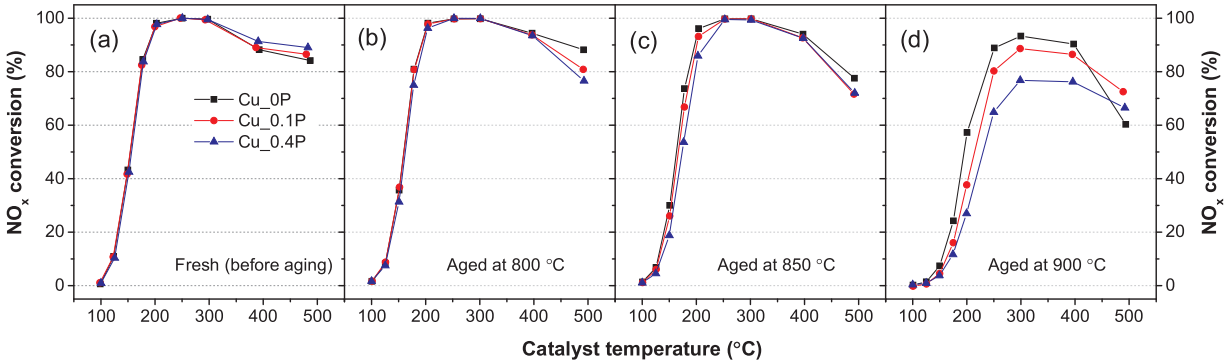

Fig. 7. NO_x conversion of standard NH_3-SCR over the fresh and P-impregnated Cu-SSZ-13: before aging (a), and after aging at 800 °C (b), 850 °C (c) and 900 °C (d). Gas conditions for aging: 8 vol.% O_2, 5 vol.% H_2O and balance Ar at 22,100 h^{-1}. Gas conditions for SCR reaction: 400 ppm NH_3, 400 ppm NO, 8 vol.% O_2, 5 vol.% H_2O and balance Ar at 22,100 h^{-1}.

poisoning (Fig. S4d).

In order to gain insight into the role of phosphorus on the changes of active sites on Cu-SSZ-13 catalysts caused by hydrothermal aging, ex-situ DRIFTS and in-situ NO-adsorption DRIFTS were performed on fresh and aged catalysts. Prior to ex-situ DRIFTS measurements, the catalysts were dehydrated and activated with 8 vol.% O_2 in Ar at 500 °C for 30 min and then cooled with same gas flow to 30 °C. After stabilizing at the same temperature in Ar flow, the IR spectra of the dehydrated catalysts were acquired. The results are shown in Fig. 8a. All spectra of fresh catalysts displayed peaks at around 3733, 3660 and 3616/3576 cm^{-1}, which can be assigned to the −OH vibrational bands that are related to silanol (Si−OH), copper ion-related hydroxyl $[Cu^{2+}(OH)^-]^+$ and zeolitic (Al−OH) groups (Brønsted acidic −OH groups) [18,59,60]. It can be seen in the figure that the intensities of those vibration bands on the spectra of hydrothermally aged catalysts decreased dramatically. The −OH vibrational bands at 3733 and 3660 cm^{-1}, in particular, remained while the bands at 3616 and 3576 cm^{-1} almost disappeared, which indicates that a complete loss of Brønsted acidic groups caused by severe dealumination processes occurred on the catalysts after successively aging at 800, 850 and 900 °C A similar phenomenon has also been reported by Luo et al. [18]. No significant differences were seen on the spectra of non-poisoned catalyst (Cu_0 P) and P-poisoned catalysts (Cu_0.1 P, and Cu_0.4 P), which is likely due to the relatively low loadings of P in the catalysts (0.26 and 1.21 wt.%, respectively).

The in-situ DRIFTS of NO adsorption were performed at 30 °C with 500 ppm NO in Ar. The IR spectra were acquired every 1 min, and the spectra after 60 min are shown in Fig. 8b. Since all catalysts were pretreated with 8 vol.% O_2 in Ar at 500 °C for 30 min and no adsorption bands in 1820–1780 cm^{-1} were observed, the existence of Cu^+ species was excluded. All the fresh catalysts show adsorption bands at 1946 + 1922 cm^{-1} and 1909 + 1880 cm^{-1}, which can be associated with the NO adsorbed on Cu^{2+} sites close to 6-MRs and 8-MRs [61,62]. Interestingly, those spectra show similar relative intensities, which suggests that P poisoning, at these poisoning levels, does not significantly impact the NO adsorption on the copper sites. This may also explain why the non-poisoned and P-poisoned Cu-SSZ-13 perform similarly in SCR reaction in the low reaction temperature region (< 300 °C). After successively aging at 800, 850 and 900 °C, the adsorption bands at 1946 + 1922 cm^{-1} disappeared from the IR spectra of aged catalysts, and the bands at 1909 + 1880 cm^{-1} shifted somewhat to 1911 + 1882 cm^{-1}. The relative intensities of the bands at 1911 + 1882 cm^{-1} changed significantly. In particular, the relative intensity of the band at 1882 cm^{-1} decreased with an increase in the level of P-poisoning, which indicates that the presence of phosphorus species has an impact on the chemical environment of copper species.

To discover the influence of hydrothermal aging on the structures of non-poisoned and P-poisoned Cu-SSZ-13, XRD and solid-state NMR

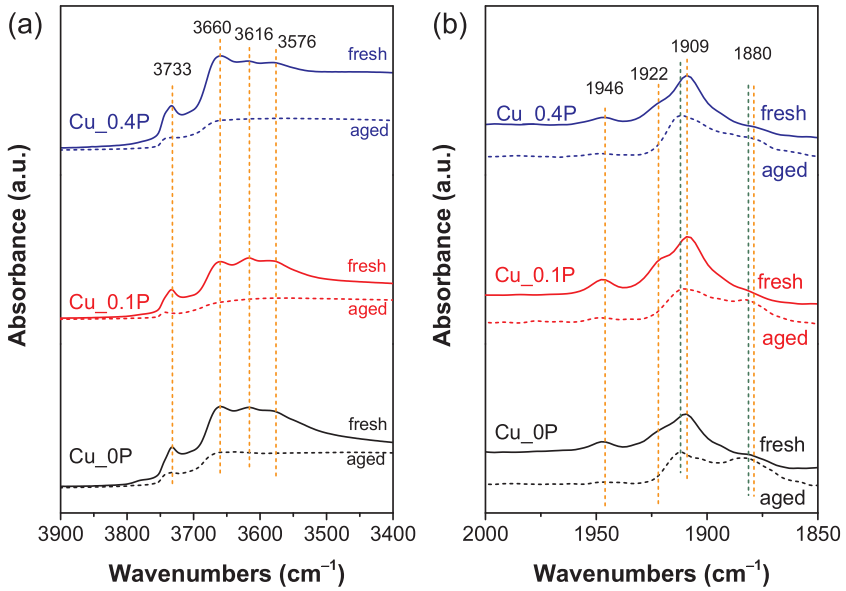

Fig. 8. (a) Ex-situ DRIFT spectra of Cu_0 P, Cu_0.1 P and Cu_0.4 P in the −OH bond vibration region. (b) In-situ DRIFT spectra of Cu_0 P, Cu_0.1 P and Cu_0.4 P after 60 min of NO adsorption. Aged catalyst denotes samples that were hydrothermally aged at 900 °C.

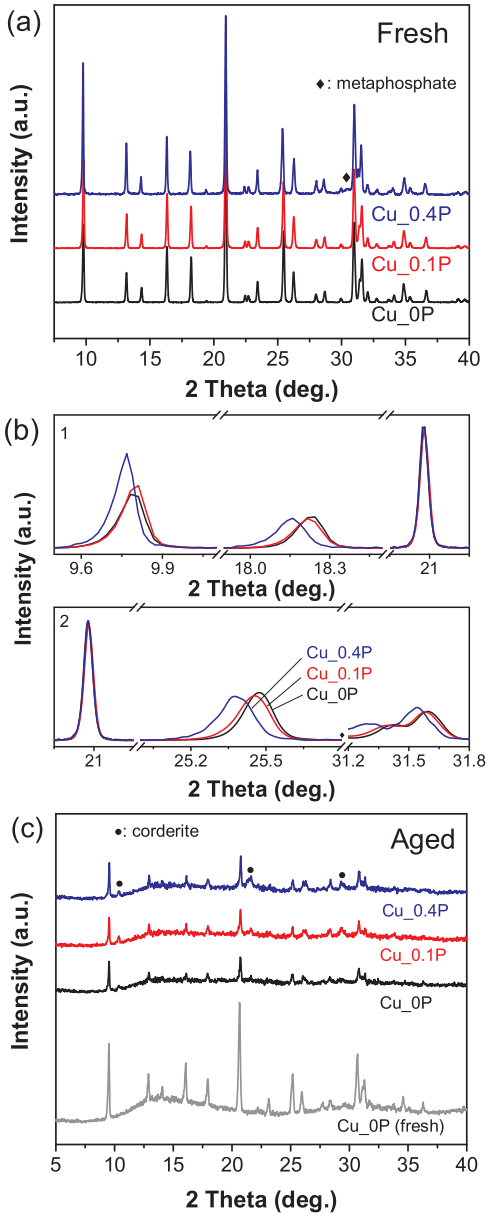

Fig. 9. XRD patterns of the non-poisoned and P-poisoned Cu-SSZ-13: (a) before aging (the unmarked peaks correspond to CHA phases), (b) zoom-in area 1 and 2 from (a), (c) after hydrothermally aging at 900 °C (fresh Cu_0 P as reference).

measurements were used to gain insight into the long-range order and short-range order, respectively. The obtained XRD patterns of the samples before aging are shown in Fig. 9a. All the samples can be identified by a CHA structure (Fig. 9a). A weak peak was observed at around 30.5°, which can be related to metaphosphate [63]. To gain further insight into the influence of phosphorus on the structure of Cu-SSZ-13, all the intensities of the diffractograms were normalized to the main characteristic peak at 20.9°, as shown in Fig. 9b. This clearly revealed that some phases shifted to the lower degrees (e.g. 9.7°, 18.5°, 25.5° and 31.5°), which means the distances between lattice planes in the zeolite framework have expanded according to Bragg's Law ($n\lambda = 2d \sin\theta$). This, in turn, implies that some of the phosphorus species are likely inside the zeolite framework.

To further examine hydrothermal aging on the structures of fresh and P-poisoned catalysts, small amounts of powders were scraped from aged monolith samples. Only about 10 mg of each sample was loaded on a polymer sample holder for the measurements, which means that the aged samples had much weaker diffractogram intensities than the fresh samples (about 100 mg was used). The XRD patterns of the aged samples are shown in Fig. 9c. Cu_0 P was measured using 10 mg of catalyst (Fig. 9c) to compare with the intensity measured with 100 mg (Fig. 9a). As expected, after hydrothermal aging at three-temperature steps (800, 850, 900 °C), significant decreases in peak intensities were clearly observed on the aged samples, which indicates a loss of crystalline CHA structure due to dealumination. Similar results have been reported in the literature [17,20,36]. Although shifts in CHA-characteristic peaks have been observed in some studies [18,19], this phenomenon was not observed in this work. The humps between 10 to 20° in the background (see Fig. 9c) can be related to the polymer sample holder, as such a hump was not observed when the measurement was performed on a special sample holder with zero background (Fig. S5a). Several peaks were observed on the diffractograms (marked with '●') that originated from the diffraction of cordierite impurities introduced when the monoliths were scraped (Fig. S5b).

The ss-NMR spectra of ^{27}Al for non-poisoned and P-poisoned SSZ-13 samples as fresh and aged are shown in Fig. 10a. Chemical shifts (δ) in the fresh samples of 57 ppm and 14 ppm can be clearly observed, and they can be assigned to the Al with tetrahedral (AlO_4) and octahedral coordinations (AlO_6) in the zeolite framework, respectively [19,21,43,64]. Since all the spectra were normalized to their sample weights and the number of accumulated scans, the intensities of δ 57 ppm and δ 14 ppm on Cu_0.1 P and Cu_0.4 P were almost the same as those for Cu_0 P, which indicates that P poisoning causes negligible changes to the main framework. In addition, $\delta - 2$ ppm, which is attributed to Al with octahedral coordination (AlO_6) in the extra zeolite framework [64], is not observed for Cu_0 P and becomes visible for Cu_0.1 P and Cu_0.4 P. This chemical shift is not likely due to the dealumination caused by the preparation of P-poisoned Cu-SSZ-13,

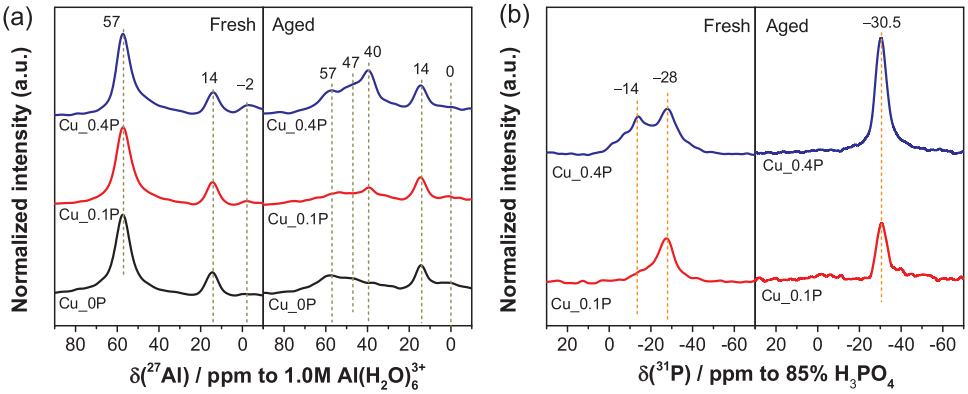

Fig. 10. (a) ^{27}Al ss-NMR of Cu_0 P, Cu_0.1 P and Cu_0.4 P. (b) ^{31}P ss-NMR of Cu_0.1 P and Cu_0.4 P. Fresh and Aged refer to the sample before and after hydrothermal aging at 900 °C, respectively. All the spectra were normalized to their sample weights and scan numbers and plotted using the same scales.

according to our previous studies. Those studies examined the hydrothermal aging of Cu-SSZ-13 catalysts, and negligible changes on $\delta -2$ ppm were observed [20]. To gain better understanding of this feature, an ^{27}Al NMR spectrum of H-SSZ-13 was recorded, and $\delta -2$ ppm could also be observed, as shown in Fig. S6. The disappearance of this feature on Cu_0 P is more likely due to the shield effect by the paramagnetic field of the ion-exchanged Cu ions at the zeolite cages. A similar phenomenon has also been observed in the literature [15,65]. After P poisoning, this feature re-emerged on Cu_0.1 P and Cu_0.4 P, which is possibly due to the paramagnetic Cu-ions being in the vicinity of phosphorus species.

Significant changes in the spectra of the samples after hydrothermal aging were observed. Although the intensities of δ 14 ppm remained for all samples, the intensities of δ 57 ppm dropped substantially. A shoulder peak emerged at δ 47 ppm, which can be related to the four-coordinated Al in the extra framework [66]. The δ 40 ppm that can be assigned to the 4-coordinated (tetrahedral) Al in aluminophosphate ($AlPO_4$) [67,68] were only observed on the aged Cu_0.1 P and Cu_0.4 P. The intensity of this feature increased with level of P poisoning, which indicates that phosphorus induced the formation of $AlPO_4$ during hydrothermal aging.

The ^{31}P ss-NMR spectra were measured for fresh and hydrothermally aged Cu_0.1 P and Cu_0.4 P and the results are shown in Fig. 10b. The $\delta -28$ ppm and $\delta -14$ ppm were observed for both fresh (P-poisoned) samples. The $\delta -28$ ppm is generally assigned to the 4-coordinated P (tetrahedral) in $P(OAl)_4$ [68–74], which indicates the formation of a localized aluminium-phosphate phase inside zeolite cages. This is likely related to the expanded distances between the lattice planes in the zeolite framework, as disclosed in the XRD study (Fig. 9b). It is also in good agreement with the observation of partial matchings of P and Al in the elemental mappings, as shown in Fig. 2. However, the assignment of $\delta -14$ ppm seems to be unclear in the literature. For silicoaluminophosphates, $\delta -14$ ppm is often assigned to the phosphorus coordinated with the adsorbed H_2O ($P(OAl)_x$ $(H_2O)_y$) [67,69]. On the other hand, Corma et al. have assigned this chemical shift to the short-chain polyphosphates on the H_3PO_4-modified Zeolite Y [75]. However, as disclosed in XPS and XRD studies (Fig. 1 and Fig. 9a), P species are mainly in the form of metaphosphates. For Cu-containing metaphosphate glasses, $\delta -14$ ppm is also proposed to be the formation of P—O—Cu linkage [76]. This assignment is highly possible as the intensity of $\delta -14$ ppm was found to increase with level of P poisoning as is supported by results of EDX-mapping, UV–vis DRS and H_2-TPR, which demonstrated a strong interaction between phosphorus and copper species. This assignment also explains that the re-emerging of δ_{Al} −2 ppm on Cu_0.1 P and Cu_0.4 P is possibly caused by the transformation of the Al—O—Cu linkage to a P—O—Cu linkage. After hydrothermal aging, $\delta -14$ ppm was found to disappear and $\delta -28$ ppm shifted to −30.5 ppm with a simultaneous increased intensity, which indicates that the phosphorus coordination had transformed from partially Cu-coordination and partially Al-coordination to completely Al-coordination.

Based on the above results, we propose that the non-poisoned and P-poisoned Cu-SSZ-13 catalysts undergo two different deactivation mechanisms, which are summarized in Scheme 1. (1) Hydrothermal aging of the non-poisoned Cu-SSZ-13 catalyst causes dealumination and produces Al species such as Al_2O_3 and $Al(OH)_3$, which are commonly observed in the literature [19,36]. It is also suggested that the formation of $Al(OH)_3$ likely hinders the dealumination process [14]. Therefore, the SCR activity of the aged Cu-SSZ-13 decreases only to a minor extent (mild deactivation). (2) Hydrothermally aging the P-poisoned Cu-SSZ-13 catalyst also causes dealumination and produces Al species such as Al_2O_3 and $Al(OH)_3$. However, the presence of phosphorus induces the extensive formation $AlPO_4$ and accelerates the collapse of the zeolite framework. Thus, the SCR activity decreases to a relatively large extent (severe deactivation).

4. Conclusions

The influence of phosphorus on the catalytic activity and hydrothermal stability of Cu-SSZ-13 SCR catalysts was studied by controlling the levels of P poisoning (0.1 and 0.4 mmol g^{-1}) using incipient wetness impregnation with an $(NH_4)_2HPO_4$ aqueous solution. The non-poisoned and P-poisoned catalysts were well characterized to probe the copper-phosphorus interaction (XPS, EDX-mapping, UV–vis DRS and H_2-TPR) and we correlated this to their catalytic activities in ammonia oxidation, NO oxidation and standard ammonia-SCR reactions. The non-poisoned and P-poisoned catalysts were successively aged in hydrothermal conditions (8 vol.% O_2, 5 vol.% H_2O in Ar; 800, 850 and 900 °C). Both fresh and aged catalysts were characterized with DRIFTS, XRD and ^{27}Al and ^{31}P ss-NMR spectroscopies to investigate the changes in active sites (Brønsted acid and copper sites) and zeolite structure (long-range and short-range orders) and to reveal the influence of phosphorus on the mechanism of catalyst deactivation via hydrothermal aging.

Three types of phosphorus species on the catalyst surface were identified using XPS analysis: phosphorus oxide (P_2O_5), metaphosphate (PO_3^-) and phosphate (PO_4^{3-}). Metaphosphate was found to be the main compound among those phosphorus species (relative concentrations of 42% for Cu_0.1 P and 55% for Cu_0.4 P), which was also detected using XRD. EDX-mapping results show that P-species deposit on Cu sites, indicating large possibility of copper-phosphorus interaction. Further characterization measurements, such as UV–vis DRS and H_2-TPR, were conducted to gain insight into the interaction between phosphorus and copper sites. The results of UV–vis DRS demonstrate that phosphorus strongly impacts the Cu electronic transition property and charge transfer processes. The results of H_2-TPR illustrate that P poisoning enforces the shift of the Cu reduction peaks to higher temperatures and a partial reduction of Cu^{2+} to Cu°. It is estimated that about 24% and 46% of copper in Cu_0.1 P and Cu_0.4 P catalysts have this interaction with phosphorus, and it mainly occurs on the copper sites close to 8-MRs. The copper-phosphorus interaction is likely due to the formation of a P—O—Cu linkage, as determined with ^{27}Al and ^{31}P ss-NMR. Phosphorus also interacts with the zeolite framework by forming the localized aluminium-phosphate phase ($AlPO_4$), as determined with ^{27}Al and ^{31}P ss-NMR. As reflected in the catalytic activities, the P-poisoning effects on ammonia-TPD, ammonia oxidation and NO oxidation reactions are much more severe than on standard ammonia-SCR reaction.

The most important finding in this work is that phosphorus-poisoning lowers the hydrothermal stability of Cu-SSZ-13. The results of ex-situ DRIFTS and in-situ NO-adsorption DRIFTS reveal the losses of Brønsted acid and copper active sites. The relative intensity of the band at 1882 cm^{-1} decreases with an increase in the level of P poisoning, indicating that the chemical environments (i.e. the zeolite framework and phosphorus species) of copper species on non-poisoned and P-poisoned Cu-SSZ-13 catalysts are changed by means of two different paths during the hydrothermal aging processes. Further, the XRD study shows dramatic losses of the chabazite structure for both non-poisoned and P-poisoned Cu-SSZ-13 catalysts. Results of ^{27}Al and ^{31}P ss-NMR reveal that phosphorus induces an extensive formation of $AlPO_4$ that accelerates the collapse of the chabazite framework. Based on our results, we propose that the deactivation of non-poisoned and P-poisoned Cu-SSZ-13 catalysts follows two different dealumination paths during hydrothermal aging.

Acknowledgements

This study was performed at the Division of Chemical Engineering and the Competence Centre for Catalysis, Chalmers University of Technology. The financial support of Cummins Inc. and the Swedish Research Council (642-2014-5733) are gratefully acknowledged. The Swedish NMR Centre is acknowledged for spectrometer time.

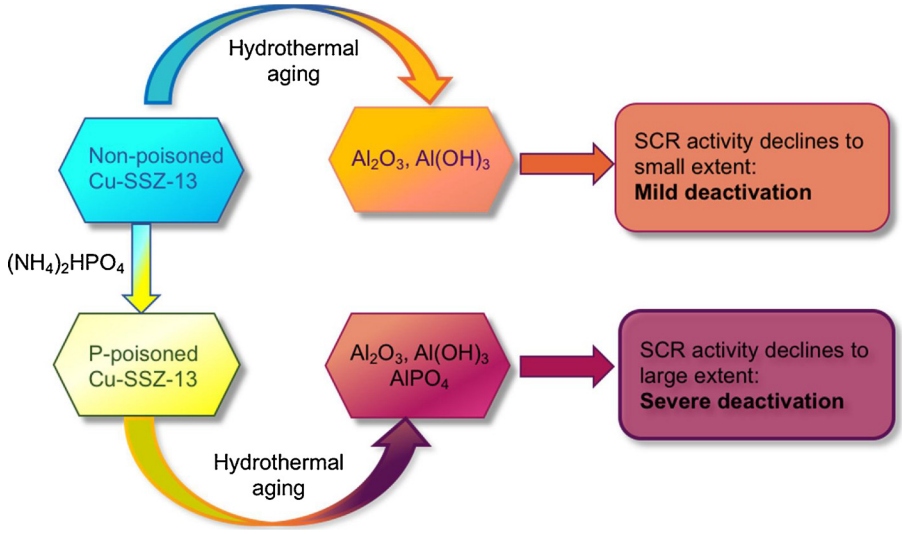

Scheme 1. Dealumination mechanisms for non-poisoned and P-poisoned catalysts.

Appendix A. Supplementary data

Supplementary material related to this article can be found, in the online version, at doi:https://doi.org/10.1016/j.apcatb.2018.08.082.

References

[1] J.H. Li, Y. Peng, H.Z. Chang, X. Li, J. Crittenden, J.M. Hao, Front. Environ. Sci. Eng. 10 (2016) 413–427.
[2] S. Brandenberger, O. Krocher, A. Tissler, R. Althoff, Catal. Rev.-Sci. Eng. 50 (2008) 492–531.
[3] Q.H. Yan, R.Y. Yang, Y.L. Zhang, A. Umar, Z.G. Huang, Q. Wang, Environ. Prog. Sustain. 35 (2016) 1061–1069.
[4] M.P. Ruggeri, I. Nova, E. Tronconi, J.E. Collier, A.P.E. York, Top. Catal. 59 (2016) 875–881.
[5] I. Bull, R.S. Boorse, W.M. Jaglowski, G.S. Koermer, A. Moini, J.A. Patchett, W.-M. Xue, P. Burk, J.C. Dettling, M.T. Caudle, U.S. Patent, 2009/7,601,662 B2, 2009.
[6] S.T. Korhonen, D.W. Fickel, R.F. Lobo, B.M. Weckhuysen, A.M. Beale, Chem. Commun. 47 (2011) 800–802.
[7] U. Deka, A. Juhin, E.A. Eilertsen, H. Emerich, M.A. Green, S.T. Korhonen, B.M. Weckhuysen, A.M. Beale, J. Phys. Chem. C 116 (2012) 4809–4818.
[8] U. Deka, I. Lezcano-Gonzalez, S.J. Warrender, A.L. Picone, P.A. Wright, B.M. Weckhuysen, A.M. Beale, Microporous Mesoporous Mater. 166 (2013) 144–152.
[9] U. Deka, I. Lezcano-Gonzalez, B.M. Weckhuysen, A.M. Beale, ACS Catal. 3 (2013) 413–427.
[10] E. Borfecchia, K.A. Lomachenko, F. Giordanino, H. Falsig, P. Beato, A.V. Soldatov, S. Bordiga, C. Lamberti, Chem. Sci. 6 (2015) 548–563.
[11] F. Gao, D.H. Mei, Yl. Wang, J. Szanyi, C.H.F. Peden, J. Am. Chem. Soc. 139 (2017) 4935–4942.
[12] C. Paolucci, I. Khurana, A.A. Parekh, S.C. Li, A.J. Shih, H. Li, J.R. Di Iorio, J.D. Albarracin-Caballero, A. Yezerets, J.T. Miller, W.N. Delgass, F.H. Ribeiro, W.F. Schneider, R. Gounder, Science 357 (2017) 898–903.
[13] F. Gao, J.H. Kwak, J. Szanyi, C.H.F. Peden, Top. Catal. 56 (2013) 1441–1459.
[14] A.M. Beale, F. Gao, I. Lezcano-Gonzalez, C.H.F. Peden, J. Szanyi, Chem. Soc. Rev. 44 (2015) 7371–7405.
[15] J.H. Kwak, D. Tran, S.D. Burton, J. Szanyi, J.H. Lee, C.H.F. Peden, J. Catal. 287 (2012) 203–209.
[16] L. Ma, Y.S. Cheng, G. Cavataio, R.W. McCabe, L.X. Fu, J.H. Li, Chem. Eng. J. 225 (2013) 323–330.
[17] Y.J. Kim, J.K. Lee, K.M. Min, S.B. Hong, I.S. Nam, B.K. Cho, J. Catal. 311 (2014) 447–457.
[18] J.Y. Luo, H.M. An, K. Kamasamudram, N. Currier, A. Yezerets, T. Watkins, L. Allard, SAE Int. J. Engines 8 (2015) 1181–1186.
[19] W.K. Su, Z.G. Li, Y. Peng, J.H. Li, Phys. Chem. Chem. Phys. 17 (2015) 29142–29149.
[20] K. Leistner, A. Kumar, K. Kamasamudram, L. Olsson, Catal. Today 307 (2018) 55–64.
[21] I. Lezcano-Gonzalez, U. Deka, H.E. van der Bij, P. Paalanen, B. Arstad, B.M. Weckhuysen, A.M. Beale, Appl. Catal. B 154 (2014) 339–349.
[22] C. Fan, Z. Chen, L. Pang, S.J. Ming, C.Y. Dong, K.B. Albert, P. Liu, J.Y. Wang, D.J. Zhu, H.P. Chen, T. Li, Chem. Eng. J. 334 (2018) 344–354.
[23] L. Ma, W.K. Su, Z.G. Li, J.H. Li, L.X. Fu, J.M. Hao, Catal. Today 245 (2015) 16–21.
[24] T. Zhang, F. Qiu, J.H. Li, Appl. Catal. B 195 (2016) 48–58.
[25] L. Olsson, K. Wijayanti, K. Leistner, A. Kumar, S.Y. Joshi, K. Kamasamudram, N.W. Currier, A. Yezerets, Appl. Catal. B 183 (2016) 394–406.
[26] J.Y. Luo, D. Wang, A. Kumar, J.H. Li, K. Kamasamudram, N. Currier, A. Yezerets, Catal. Today 267 (2016) 3–9.
[27] K. Wijayanti, K.P. Xie, A. Kumar, K. Kamasamudram, L. Olsson, Appl. Catal. B-Environ. 219 (2017) 142–154.
[28] K. Wijayanti, K. Leistner, S. Chand, A. Kumar, K. Kamasamudram, N.W. Currier, A. Yezerets, L. Olsson, Catal. Sci. Technol. 6 (2016) 2565–2579.
[29] K.P. Xie, K. Leistner, K. Wijayanti, A. Kumar, K. Kamasamudram, L. Olsson, Catal. Today 297 (2017) 46–52.
[30] L. Chen, H. Falsig, T.V.W. Janssens, H. Grönbeck, J. Catal. 358 (2018) 179–186.
[31] L. Chen, J. Jansson, M. Skoglundh, H. Grönbeck, J. Phys. Chem. C 120 (2016) 29182–29189.
[32] D. Jo, T. Ryu, G.T. Park, P.S. Kim, C.H. Kim, I.S. Nam, S.B. Hong, ACS Catal. 6 (2016) 2443–2447.
[33] T. Ryu, N.H. Ahn, S. Seo, J. Cho, H. Kim, D. Jo, G.T. Park, P.S. Kim, C.H. Kim, E.L. Bruce, P.A. Wright, I.S. Nam, S.B. Hong, Angew. Chem. Int. Ed. 56 (2017) 3256–3260.
[34] S.J. Eaton, B.G. Bunting, T.J. Toops, K. Nguyen, The Roles of Phosphorus and Soot on the Deactivation of Diesel Oxidation Catalysts, SAE International, 2009.
[35] S. Andonova, E. Vovk, J. Sjöblom, E. Ozensoy, L. Olsson, Appl. Catal. B 147 (2014) 251–263.
[36] S. Han, Q. Ye, S.Y. Cheng, T.F. Kang, H.X. Dai, Catal. Sci. Technol. 7 (2017) 703–717.
[37] G.L. Shoemaker, J.B. Anderson, E. Kostiner, Acta Crystallogr. B B33 (1977) 2969–2972.
[38] C.E. Bamberger, E.D. Specht, L.M. Anovitz, J. Am. Ceram. Soc. 80 (1997) 3133–3138.
[39] T. Kanerva, V. Kroger, K. Rahkamaa-Tolonen, M. Vippola, T. Lepisto, R.L. Keiski, Top. Catal. 45 (2007) 137–142.
[40] S.K. Matam, M.A. Newton, A. Weidenkaff, D. Ferri, Catal. Today 205 (2013) 3–9.
[41] M.J. Rokosz, A.E. Chen, C.K. Lowe-Ma, A.V. Kucherov, D. Benson, M.C.P. Peck, R.W. McCabe, Appl. Catal. B-Environ. 33 (2001) 205–215.
[42] K. Wijayanti, S. Andonova, A. Kumar, J.H. Li, K. Kamasamudram, N.W. Currier, A. Yezerets, L. Olsson, Appl. Catal. B 166 (2015) 568–579.
[43] S.J. Schmieg, S.H. Oh, C.H. Kim, D.B. Brown, J.H. Lee, C.H.F. Peden, D.H. Kim, Catal. Today 184 (2012) 252–261.
[44] J.Y. Luo, H.M. An, K. Kamasamudram, N. Currier, A. Yezerets, T. Watkins, L. Allard, SAE Int. J. Engines 8 (2015), https://doi.org/10.4271/2015-4201-1022.
[45] J.F. Moulder, W.F. Stickle, P.E. Sobol, K.D. Bomben, Handbook of X-Ray Photoelectron Spectroscopy, Perkin-Elmer Corp., Eden Prairie, Minnesota, 1992.
[46] S. Shwan, J. Jansson, L. Olsson, M. Skoglundh, Appl. Catal. B-Environ. 147 (2014) 111–123.
[47] A.K.S. Clemens, A. Shishkin, P.A. Carlsson, M. Skoglundh, F.J. Martinez-Casado, Z. Matej, O. Balmes, H. Harelind, ACS Catal. 5 (2015) 6209–6218.
[48] T. Zhang, J.M. Li, J. Liu, D.X. Wang, Z. Zhao, K. Cheng, J.H. Li, AlChE J. 61 (2015) 3825–3837.
[49] N. Wilken, R. Nedyalkova, K. Kamasamudram, J. Li, N.W. Currier, R. Vedaiyan, A. Yezerets, L. Olsson, Top. Catal. 56 (2013) 317–322.
[50] J.H. Kwak, H. Zhu, J.H. Lee, C.H.F. Peden, J. Szanyi, Chem. Commun. 48 (2012) 4758–4760.
[51] J.C. Wang, Z.L. Peng, H. Qiao, H.F. Yu, Y.F. Hu, L.P. Chang, W.R. Bao, Ind. Eng. Chem. Res. 55 (2016) 1174–1182.
[52] G.V. Mamontov, O.V. Magaev, A.S. Knyazev, O.V. Vodyankina, Catal. Today 203 (2013) 122–126.
[53] C. Sepúlveda, L. Delgado, R. García, M. Melendrez, J.L.G. Fierro, I.T. Ghampson, N. Escalona, Catal. Today 279 (2017) 217–223.
[54] K. Leistner, K.P. Xie, A. Kumar, K. Kamasamudram, L. Olsson, Catal. Lett. 147

(2017) 1882–1890.
[55] C. Paolucci, A.A. Parekh, I. Khurana, J.R. Di Iorio, H. Li, J.D.A. Caballero, A.J. Shih, T. Anggara, W.N. Delgass, J.T. Miller, F.H. Ribeiro, R. Gounder, W.F. Schneider, J. Am. Chem. Soc. 138 (2016) 6028–6048.
[56] L. Olsson, K. Wijayanti, K. Leistner, A. Kumar, S.Y. Joshi, K. Kamasamudram, N.W. Currier, A. Yezerets, Appl. Catal. B 174 (2015) 212–224.
[57] A.A. Verma, S.A. Bates, T. Anggara, C. Paolucci, A.A. Parekh, K. Kamasamudram, A. Yezerets, J.T. Miller, W.N. Delgass, W.F. Schneider, F.H. Ribeiro, J. Catal. 312 (2014) 179–190.
[58] N. Wilken, K. Wijayanti, K. Kamasamudram, N.W. Currier, R. Vedaiyan, A. Yezerets, L. Olsson, Appl. Catal. B 111 (2012) 58–66.
[59] J.H. Kwak, T. Varga, C.H.F. Peden, F. Gao, J.C. Hanson, J. Szanyi, J. Catal. 314 (2014) 83–93.
[60] I. Lezcano-Gonzalez, U. Deka, B. Arstad, A. Van Yperen-De Deyne, K. Hemelsoet, M. Waroquier, V. Van Speybroeck, B.M. Weckhuysen, A.M. Beale, J. Chem. Soc. Faraday Trans. 16 (2014) 1639–1650.
[61] J. Szanyi, J.H. Kwak, H.Y. Zhu, C.H.F. Peden, Phys. Chem. Chem. Phys. 15 (2013) 2368–2380.
[62] R.Q. Zhang, J.S. McEwen, M. Kollár, F. Gao, Y.L. Wang, J. Szanyi, C.H.F. Peden, ACS Catal. 4 (2014) 4093–4105.
[63] B.S. Bae, M.C. Weinberg, J. Am. Ceram. Soc. 76 (1993) 1395–1400.
[64] Y. Zhang, H.N. Wang, R.Y. Chen, RSC Adv. 5 (2015) 67841–67848.
[65] S. Prodinger, M.A. Derewinski, Y.L. Wang, N.M. Washton, E.D. Walter, J. Szanyi, F. Gao, Y. Wang, C.H.F. Peden, Appl. Catal. B 201 (2017) 461–469.
[66] J. Rocha, S.W. Carr, J. Klinowski, Chem. Phys. Lett. 187 (1991) 401–408.
[67] A. Buchholz, W. Wang, A. Arnold, M. Xu, M. Hunger, Microporous Mesoporous Mater. 57 (2003) 157–168.
[68] C.S. Blackwell, R.L. Patton, J. Phys. Chem. 88 (1984) 6135–6139.
[69] A. Buchholz, W. Wang, M. Xu, A. Arnold, M. Hunger, Microporous Mesoporous Mater. 56 (2002) 267–278.
[70] J.G. Longstaffe, B.H. Chen, Y.N. Huang, Microporous Mesoporous Mater. 98 (2007) 21–28.
[71] M.P.J. Peeters, J.W. Dehaan, L.J.M. Vandeven, J.H.C. Vanhooff, J. Phys. Chem. 97 (1993) 5363–5369.
[72] D. Muller, E. Jahn, G. Ladwig, U. Haubenreisser, Chem. Phys. Lett. 109 (1984) 332–336.
[73] J.Z. Hu, M.Y. Hu, Z.C. Zhao, S.C. Xu, A. Vjunov, H. Shi, D.M. Camaioni, C.H.F. Peden, J.A. Lercher, Chem. Commun. 51 (2015) 13458–13461.
[74] K.R. Carduner, M.S. Chattha, H.S. Gandhi, J. Catal. 109 (1988) 37–40.
[75] A. Corma, V. Fornes, W. Kolodziejski, L.J. Martineztriguero, J. Catal. 145 (1994) 27–36.
[76] P.Y. Shih, J.Y. Ding, S.Y. Lee, Mater. Chem. Phys. 80 (2003) 391–396.